



A tracer-based algorithm for automatic generation of seafloor age grids from plate tectonic reconstructions

Krister S. Karlsen^{*}, Mathew Domeier, Carmen Gaina, Clinton P. Conrad

Centre for Earth Evolution and Dynamics, University of Oslo, Norway

ARTICLE INFO

Keywords:

Paleozoic
Seafloor age grids
Plate tectonic reconstructions
Sea level change
Oceanic lithosphere
Reconstructed bathymetry

ABSTRACT

The age of the ocean floor and its time-dependent age distribution control fundamental features of the Earth, such as bathymetry, sea level and mantle heat loss. Recently, the development of increasingly sophisticated reconstructions of past plate motions has provided models for plate kinematics and plate boundary evolution back in geological time. These models implicitly include the information necessary to determine the age of ocean floor that has since been lost to subduction. However, due to the lack of an automated and efficient method for generating global seafloor age grids, many tectonic models, most notably those extending back into the Paleozoic, are published without an accompanying set of age models for oceanic lithosphere. Here we present an automatic, tracer-based algorithm that generates seafloor age grids from global plate tectonic reconstructions with defined plate boundaries. Our method enables us to produce novel seafloor age models for the Paleozoic's lost ocean basins. Estimated changes in sea level based on bathymetry inferred from our new age grids show good agreement with sea level record estimations from proxies, providing a possible explanation for the peak in sea level during the assembly phase of Pangea. This demonstrates how our seafloor age models can be directly compared with observables from the geologic record that extend further back in time than the constraints from preserved seafloor. Thus, our new algorithm may also aid the further development of plate tectonic reconstructions by strengthening the links between geological observations and tectonic reconstructions of deeper time.

1. Introduction

The discovery of a method to determine the age of the present-day oceanic crust, using reversals of the Earth's magnetic field (Vine and Matthews, 1963), gave rise to the recognition that the seafloor is spreading, and ultimately to the development and broad acceptance of plate tectonics. In the half-century since the plate tectonic revolution, detailed age models of the present-day oceanic lithosphere have been constructed, and digital global oceanic age grids are continuously refined (Müller et al., 1997, 2008a, 2016). A wealth of information, mainly from marine geophysical data, but also from the geology of continental margins, have been used to reconstruct the extent and age distribution of oceanic lithosphere of the past, including portions that have been subducted (Müller et al., 2008b). These “paleo-seafloor age grids” present rich new opportunities for scientific inquiry, as a wide range of Earth processes can be further interrogated with the use of such age grids. Example applications include the estimation of paleobathymetry (spatial and temporal changes in ocean basin depth, which in turn is important for understanding past ocean currents and their effect on paleoclimate, e.g., Straume et al. 2019), sea level

change (Müller et al., 2008b), global seafloor heat flow (Loyd et al., 2007; Cramer et al., 2019), and the subduction volume flux, which impacts geomagnetic reversals (Hounslow et al., 2018), the thermal structure of paleo-subduction zones (Maunder et al., 2019), transport of water (Karlsen et al., 2019a) and carbon (Merdith et al., 2019) to the deep mantle, and the slab pull force on tectonic plates (Conrad and Lithgow-Bertelloni, 2004; Faccenna et al., 2012). Seafloor ages for past times are also important as a boundary condition for global mantle convection models (Gurnis et al., 2012).

Present day age grid models are based on a set of isochrons (lines defined by equal seafloor ages) constructed using information from magnetic and gravity data available at various resolutions in most oceanic basins. Ages for seafloor locations between isochrons are computed based on rotation parameters that describe the plate motions for various time intervals. The isochrons and rotation parameters are linked to a specific geomagnetic timescale, and the choice of timescales will influence the calculated values of spreading velocities. To ensure a smooth grid of ocean floor ages that maintains sharp age discontinuities at fracture zones, Müller et al. (1997) designed an algorithm where

^{*} Corresponding author.

E-mail address: k.s.karlsen@geo.uio.no (K.S. Karlsen).

they first created a set of densely interpolated isochrons along plate flow lines, and then used a minimum curvature routine to obtain age values on a regular grid. This method for reconstructing seafloor age from present-day seafloor age data and a plate kinematic model is time-consuming and requires significant human input, and consequently may be subjective or introduce errors. Because of this, seafloor ages are usually only determined after a plate reconstruction model has been finalized; they have not previously been computed “on the fly” from the plate kinematic model itself.

The mid-ocean ridges constitute the locus of seafloor generation through time, while plate kinematics define the seafloor’s subsequent journey until its destruction at a subduction zone. Thus, global plate tectonic reconstructions that define the motions of the plates and the locations and types of plate boundaries (see Gurnis et al. 2012 for further descriptions of such models) also implicitly define the age and structure of oceanic basins. Global plate tectonic models with dynamic plate boundaries (Gurnis et al., 2012) have been constructed back into the mid-Paleozoic (410 Ma; Domeier and Torsvik 2014, Matthews et al. 2016), but published paleo-seafloor age grids are only available globally for the last 250 Ma (Müller et al., 2019). This timing discrepancy has, partly, occurred because the reconstruction of global paleo-seafloor age grids from a plate tectonic reconstruction presents a tedious and labor intensive task in the absence of an automatic method. Moreover, these reconstructions are subject to continuous changes as new geological information becomes available. It follows that an automatic and more efficient method for seafloor age determination is needed to allow the use of plate tectonic reconstructions to better decipher Earth’s processes and dynamics through time. An automatic method also allows detecting inconsistencies in kinematic models, which would help to improve them. In this study we present such an automatic method for generating seafloor age grids, and introduce a specific implementation of it as an open-source Python code called *Tracer Tectonics* (or *TracTec*) (Karlsen et al., 2019b).

2. Methods

The algorithm specifically acts upon “self-closing” plate polygon models (Gurnis et al., 2012) that evolve over time from a set of dynamically evolving plate boundaries. Conventionally, such models comprise a *rotation file*, a *plate boundary file* and a *continent polygon file*. The rotation file (*.rot file) represents a series of finite rotations that describe the time-dependent motions of each plate, which are identified by their associated Plate ID. The motion of plates by rotations about Euler poles (e.g. Greiner 1999), and the surface velocity field (Fig. 1A), can be described at each point in time $t \in [0, T]$, where $t = 0$ defines the present-day and $t = T$ is the earliest point in time for which the plate reconstruction is defined. We prefer to refer to t as time, rather than age, to avoid confusion with the age of the seafloor.

The time-dependent motions described by the *.rot file can be used to reconstruct any framework of points, polylines (continuous lines composed of one or more line segments) and polygons that are ascribed Plate IDs defined in the *.rot file. The continent polygon file, for example, contains static polygons (tagged with metadata Plate IDs) that represent blocks of continental lithosphere that can be reconstructed and passively rotated through time by the *.rot file. The plate boundary file contains the polylines that are used (in conjunction with the *.rot file) to reconstruct the dynamic plate polygons at any time t , following the method of Gurnis et al. (2012). These polylines are associated with metadata tags that identify the type of plate boundary that they represent; in the following, we will be interested in those that are either identified as mid-ocean ridge or subduction zone (Fig. 1B).

We divide the computational approach for generating seafloor age grids from kinematic plate models into three modules: *preprocessing*, *main algorithm* and *post-processing* (Fig. 2). The Python scripts that we developed for each of these modules are part of the *TracTec*-package, and can be downloaded from: <http://doi.org/10.5281/zenodo.368754> 8.

2.1. Preprocessing

As the time-dependent spatial distribution of mid-ocean ridges and subduction zones, together with plate kinematics, dictates the age of the ocean floor, we need to extract these properties from a given full-plate model and output them in a convenient format. To accomplish this, we use *pyGPlates*, which is a Python-based scripting interface to *GPlates* (Boyden et al., 2011) that allows for easy automation of such tasks. For each point in time t we extract plate boundaries labeled as mid-ocean ridges from the plate boundary file, and re-sample these polyline segments at user-defined intervals Δ_R (50 km by default). Subduction zone plate boundary segments are extracted and sampled in the same manner ($\Delta_S = 20$ km by default).

2.2. Main algorithm

To simulate and track the journey of oceanic lithosphere through space and time, from its creation along a mid-ocean ridge until its destruction at a subduction zone, we use tracers. These are numerical particles on which quantities of interest are tracked. The essential property we want to track with the tracers is the age of the oceanic lithosphere. A secondary property we track is the Plate ID associated with each tracer, i.e. the plate to which each tracer currently belongs. We track Plate IDs to determine when a tracer crosses a plate boundary (recognized by a change in its associated Plate ID), which in turn is useful to detect subduction of tracers. At a given time t , the number of tracers is $N_T(t)$, their positions are $\mathbf{x}_n(t)$, their ages $\tau_n(t)$, and their associated Plate IDs are $p_n(t)$, for $n = 0, 1, \dots, N_T(t) - 1$.

We break the algorithm into individual sub-steps (see below, 1–7) that are completed at every integer time-step $t \in [0, T]$, before moving on to the next. Although our algorithm is capable of operating at any arbitrary time-step, we fix the time-step size Δt to 1 Myr in accordance with the inherent temporal resolution that modern plate tectonic reconstructions are made. The use of larger time-steps would yield sparse age-grids and omit meaningful kinematic data, whereas smaller time-steps could result in erroneous behavior owing to deficiencies in the input plate model below the standard assumed temporal resolution of 1 Myr.

(1) Add tracers

At the beginning of each time-step we add tracers at intervals given by Δ_R on each side of the mid-ocean ridges (Fig. 3A). The tracers are added at a small offset distance ϵ_R (1 km by default) from the ridge to ensure that they are within the polygons that define the two spreading plates. Their initial ages $\tau_n(t)$ are set to zero. The uncertainty introduced by adding tracers at this offset distance is given by ϵ_R/v_s , where v_s is the half-spreading rate. For an average mid-ocean ridge ($v_s \sim 26$ mm/yr) $\epsilon_R/v_s \approx 0.04$ Myrs.

(2) Get tracer Plate IDs

Based on the tracers’ positions $\mathbf{x}_n(t)$, we use *pyGPlates*’ point-in-polygon algorithm to assign them their Plate IDs $p_n(t)$.

(3) Move tracers

To determine how the tracers move from t to $t + \Delta t$ (Fig. 3B–C), we use *pyGPlates* to query the *rotation file* to obtain the finite rotation associated with each tracer (which is based on their Plate IDs $p_n(t)$). Next, by applying that rotation to their current positions \mathbf{x}_n , we obtain their new positions $\mathbf{x}_n(t + \Delta t)$.

(4) Update tracer Plate IDs

Based on the tracers’ new positions $\mathbf{x}_n(t + \Delta t)$, we use *pyGPlates*’ point-in-polygon algorithm to assign them their new Plate IDs $p_n(t + \Delta t)$.

(5) Check for subduction

After having moved the tracers from $\mathbf{x}_n(t)$ to $\mathbf{x}_n(t + \Delta t)$, we check if any tracers have been subducted (Fig. 3H–I). This is accomplished by first determining which tracers have changed Plate ID by comparing $p_n(t)$ against $p_n(t + \Delta t)$. Given the sub-set of tracers that have changed

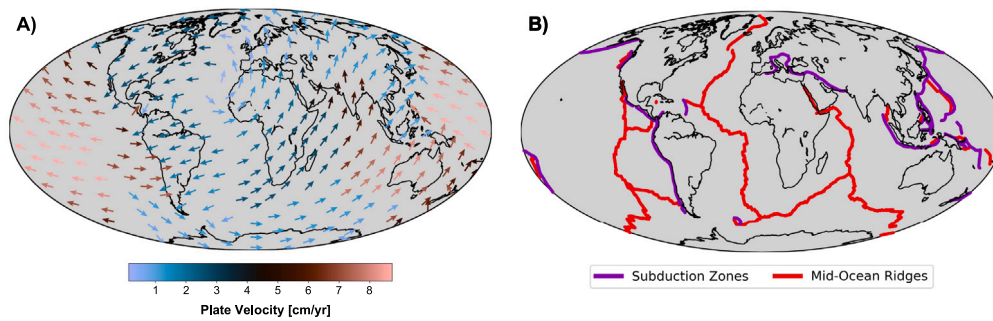


Fig. 1. Present day global surface velocity field (A) and locations of mid-ocean ridges and subduction zones (B) derived from a global plate tectonic reconstruction (Matthews et al., 2016).

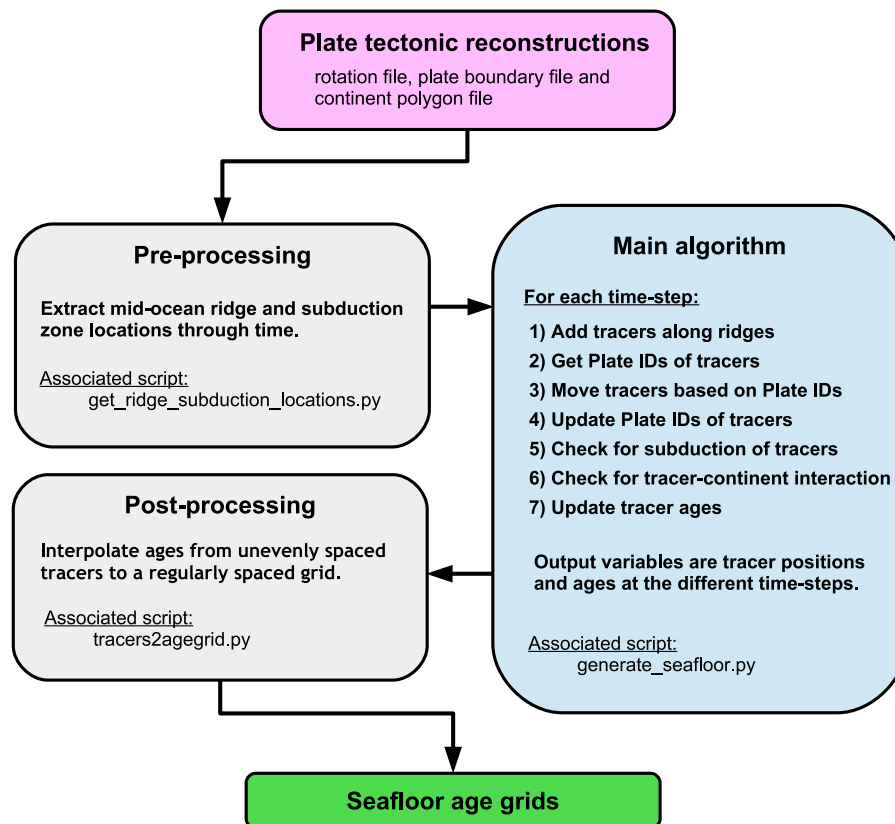


Fig. 2. Flow chart of TracTec (Karlsen et al., 2019b) showing an overview of the algorithm and the steps used to generate seafloor age grids from plate tectonic reconstructions.

Plate ID, we determine if any are within distance R_{min} of a subduction zone boundary. The default value of R_{min} is set to 100 km, which we have found to be appropriate. Any tracers that fulfill both of these criteria are considered subducted and are thus terminated at this time-step.

(6) Check for tracer–continent interaction

To ensure that tracers do not end up on continents (which could happen in nature, e.g. ophiolites, but should not happen in conventional dynamic plate polygon models, but nevertheless occurs due to inexorable flaws in such models), we delete all tracers that end up inside continent polygons (checked using pyGPlates' point-in-polygon algorithm against the continent polygon file).

(7) Update tracer ages

Before moving on to the next time-step, which practically means returning to step (1) of the algorithm, we update the age of the tracers that are left after the two filtering steps (5–6), by simply by adding Δt to their current age, obtaining $\tau_n(t + \Delta t)$.

2.3. Post-processing

The output from steps (1–7) is unevenly distributed tracer positions $\mathbf{x}_n(t)$ associated with ages $\tau_n(t)$. However, for most applications, it is convenient to express the seafloor ages on a regular grid, rather than at arbitrary points. This calls for a post-processing step that interpolates seafloor ages from tracer positions onto a regular grid. There are countless ways of doing this, ranging from simple nearest neighbor algorithms, to weighted means, to splines, etc. Depending on the application, smoothing of the resulting age grids may be preferred or required. In our online repository we provide an example of a simple post-processing script that uses GMT's linear interpolation algorithm (Wessel et al., 2013) to obtain seafloor ages on a regular grid.

The Python scripts to generate age grids based on the steps described above using Tracer Tectonics are provided in the Zenodo repository (Karlsen et al., 2019b). A summary and a general overview of the algorithm are shown in Fig. 2.

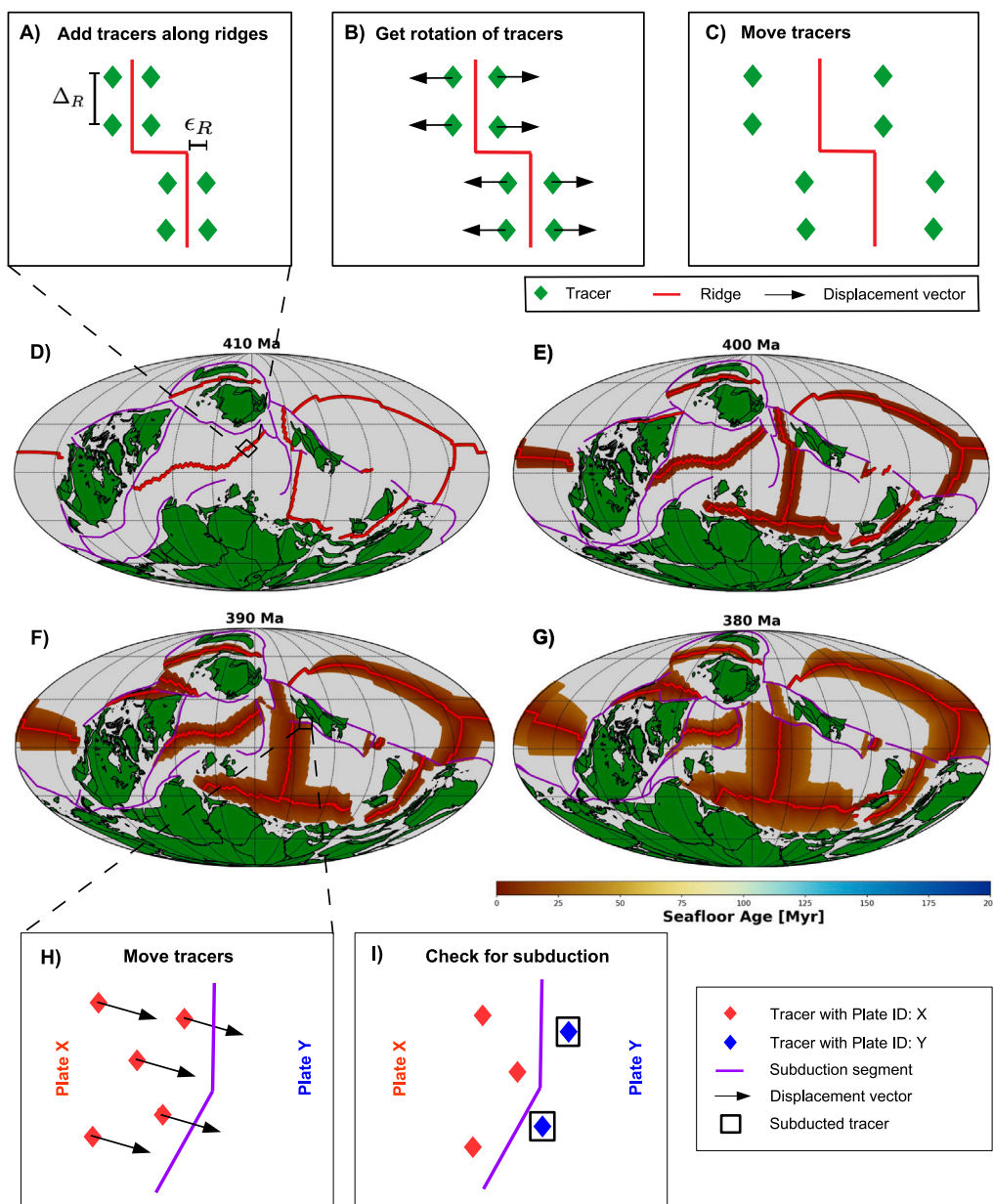


Fig. 3. Schematics illustrating how tracers are added along mid-ocean ridges (A), moved (B–C), and checked for subduction (H–I). The repeated application of these steps over time leads to an ocean basin gradually filled with tracers that track the age of the ocean floor (D–G). In this example the model of Matthews et al. (2016) is used. Note that (A–C, H–I) are not to scale.

2.4. Initial condition

Running the algorithm without any initial condition, as in the example of Fig. 3D–G, we see that it takes some tens of millions of years before the ocean basins are entirely covered by tracers. Technically, this is the time it takes for the predicted seafloor ages to result solely from the plate kinematics of the input model. Alternatively, one could apply an initial condition that incorporates some educated guess of the seafloor ages for the initial time step. This is straightforward to include in the framework presented (steps 1–7 of the main algorithm), by simply initializing $x_n(t = T)$ and $\tau_n(t = T)$. As with any time-dependent model, one should be aware of the assumptions implicit to the chosen initial condition, and its effects on the model output. For this algorithm, it is straightforward to track the effect of an applied initial condition. This can be achieved by simply tracking the fraction of initial tracers through time (Fig. S1); at some point, all the initial

tracers will be eliminated, from which point the output will no longer depend on the initial condition.

3. Discussion

3.1. Validation and benchmarking

To validate our algorithm and its implementation, we compare the seafloor age grids generated by our algorithm against published present-day seafloor age models (Benchmark #1, Fig. 4), direct point observations of present-day seafloor ages (Benchmark #2, Fig. 5) and against the time-dependent age-area distribution of the oceanic lithosphere for the last 230 Myr (Benchmark #3, Fig. 6) based on Müller et al. (2016) (hereafter 'M16').

To generate the seafloor age grids used to evaluate the performance of our algorithm (with its default settings), we employed Matthews et al. (2016) as the input plate model with the initial condition shown

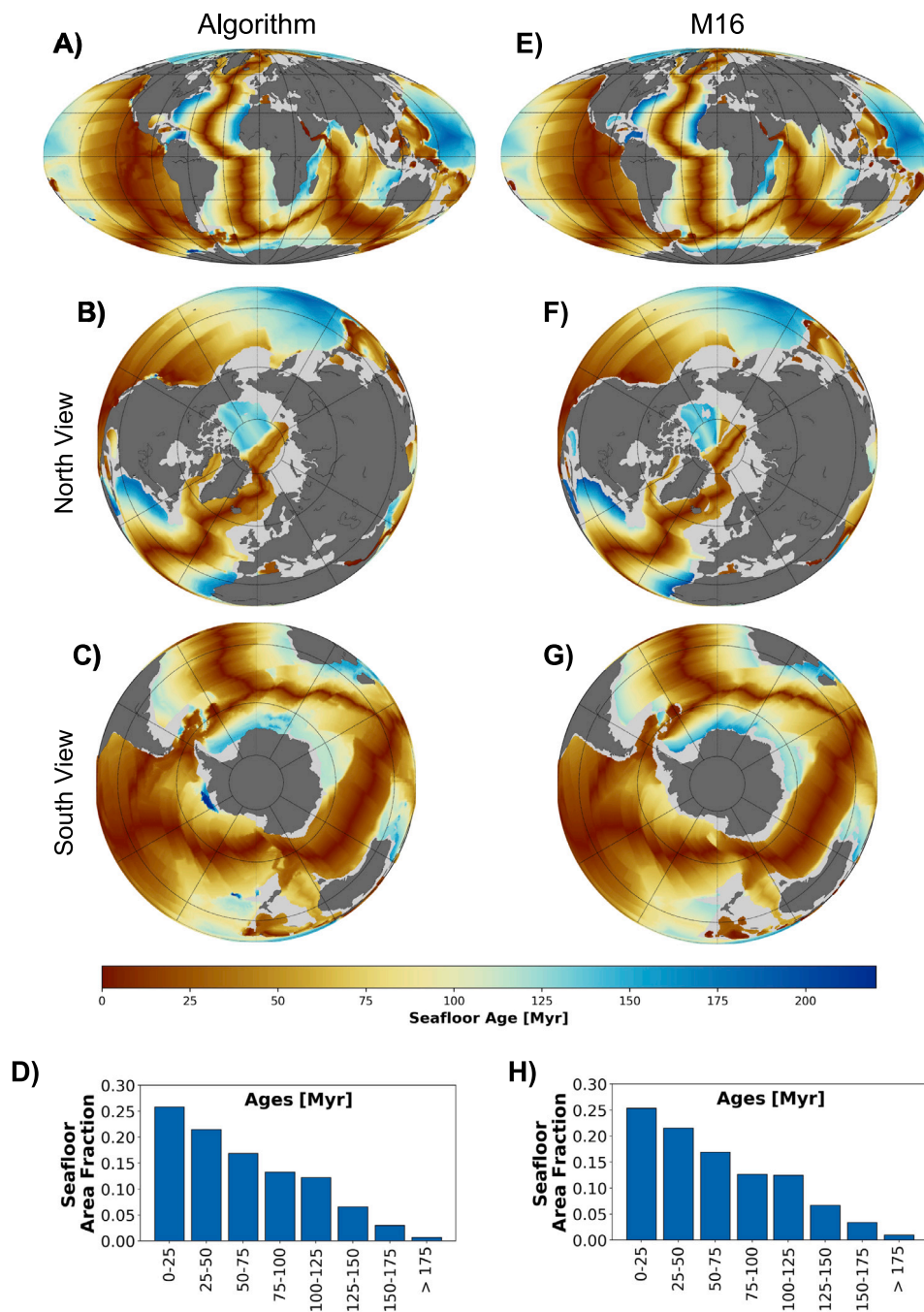


Fig. 4. Benchmark #1: Maps comparing present-day seafloor ages generated by our algorithm (A–C) to those of M16 (Müller et al., 2016) model (E–G), and their corresponding age-area distributions (D and H). The input plate model used here was Matthews et al. (2016).

in Fig. 7A. Notably, the effect of an initial condition applied at 400 Ma is very small already by 300 Ma (only 11% of the initial tracers remain), and zero at the present-day (Fig. S1). The initial condition and the age grids are available from our online repository (Karlsen et al., 2019b).

Our algorithm reproduces the present-day seafloor well (Fig. 4A–C), as can be seen from the maps comparing the resulting age grids to those of M16 (Fig. 4E–G). The characteristic triangular present-day seafloor age-area distribution (Sclater et al. 1980, Cogné and Humler 2004), which shows the fraction of the ocean floor that falls within a certain age range, is also well reproduced. On the regional scale, some minor differences can be seen, for example there are three narrow bands of artificially young seafloor branching from the Mid-Atlantic Ridge near the Caribbean and west of Iberia. These are merely consequences of the underlying plate model (Matthews et al., 2016), for which

these plate boundaries are erroneously designated as mid-ocean ridges, either at present (Fig. 1), or in the recent past. This demonstrates that a combined work-flow for developing plate tectonic reconstructions, which incorporates the generation and analysis of seafloor age grids, can reveal flaws and inconsistencies in the plate model. In the case of the aforementioned errors in the mid-Atlantic, simply re-labeling the offending boundaries as transform features and re-running the age grid algorithm addresses the issue.

To further evaluate the performance of our algorithm, we compare the generated present-day age grid against ages inferred from magnetic reversal picks (Fig. 5). This global dataset provides by far the most comprehensive, direct sources of oceanic lithosphere ages, and is available from the Global Seafloor Fabric and Magnetic Lineation (GSFML) database (Seton et al., 2014). We see that ~37% of the 101418 pick

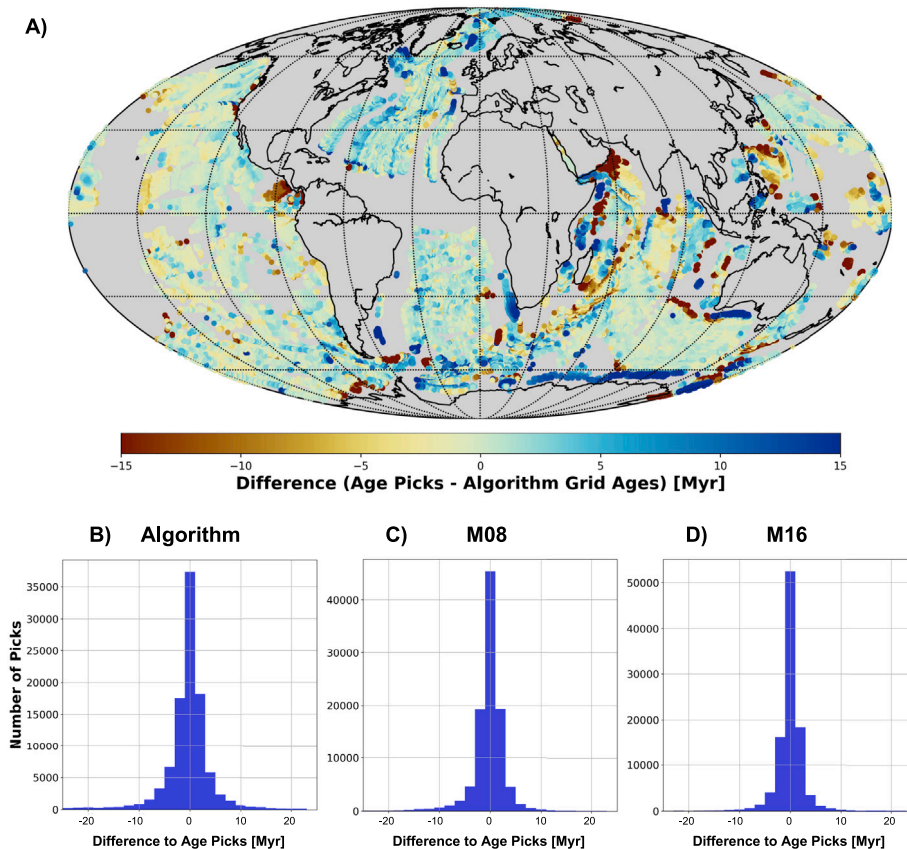


Fig. 5. Benchmark #2: Map (A) comparing the present-day age grid generated by our automatic algorithm to ages inferred from magnetic reversal picks (Seton et al., 2014). Distributions (B–D) show the number of pick ages that fall within a certain deviation from (B) our algorithm-generated age grid, (C) M08 - Müller et al. (2008a) and (D) M16 - Müller et al. (2016). The total number of pick ages is 101418.

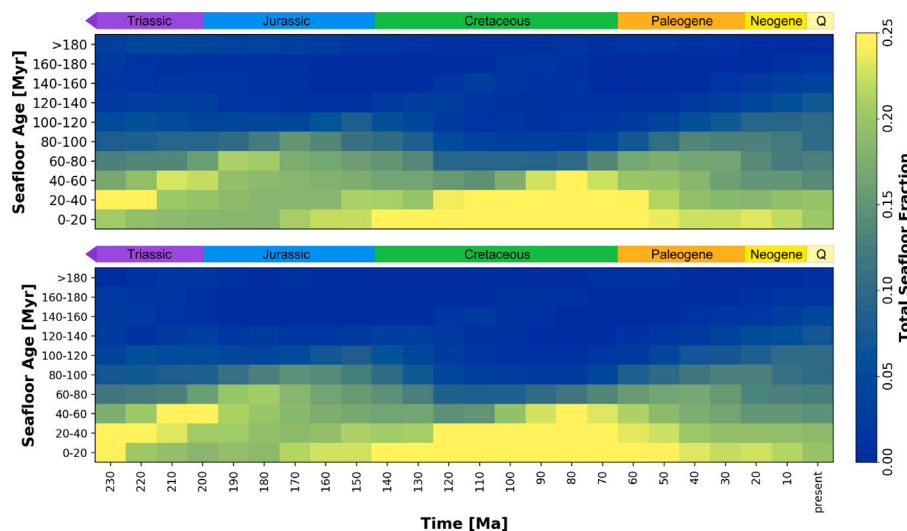


Fig. 6. Benchmark #3: Comparison of the age-area distribution of the seafloor through time for our algorithm created age grids (top) and the Müller et al. (2016) (M16) model (bottom).

ages are within ± 1 Myr of the ages from our age grids, and $\sim 84\%$ are within ± 5 Myr (Fig. 5B). These numbers are slightly higher for models of the present-day ocean floor that are based on more labor-intensive methods (described in Section 1) such as Muller et al. (2008b), for which they are $\sim 45\%$ and $\sim 92\%$ respectively (Fig. 5C), and $\sim 52\%$ and $\sim 93\%$ for M16 (Fig. 5D).

As pointed out in several studies (e.g. Becker et al. 2009, Coltice et al. 2012, Sim et al. 2016), the triangular age-area distribution of the present-day ocean floor is unlikely to be a constant feature through Earth’s history. In particular, large fluctuations are predicted to have occurred in the rates of seafloor spreading and global subduction (e.g. Hays and Pitman 1973), which should preclude a constant age-area distribution of the seafloor. Moreover, the age-area distribution of

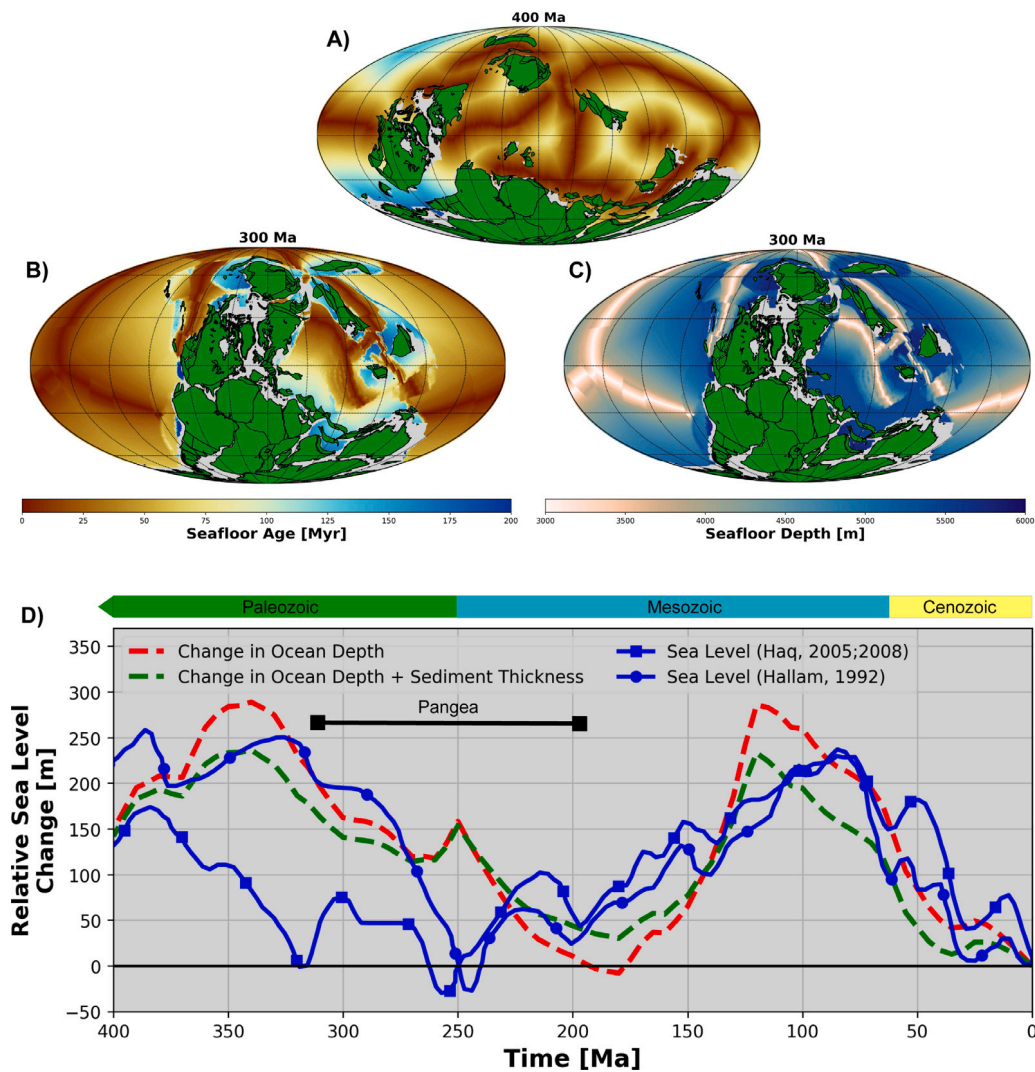


Fig. 7. Initial condition (A) used to generate seafloor age grids from the plate reconstruction of Matthews et al. (2016) from 400 Ma to the present. A snapshot at 300 Ma shows seafloor ages (B) and bathymetry (C) computed by applying the age-depth relation of Crosby and McKenzie (2009). Panels (A) and (B) use the same colorbar. From the bathymetry models we compute changes in mean ocean depth and isostatically compensate them (Pitman, 1978) to compare sea level changes relative to the present day (C, red dashed line) to Phanerozoic sea level reconstructions (C, blue lines) inferred from the sedimentary record (Hallam, 1992; Haq and Al-Qahtani, 2005; Haq and Schutter, 2008). The effect of time-variations in sediment thickness on the sea level prediction (C, green dashed line) is computed after equation 2a in Straume et al. (2019). Thick black bar shows the approximate duration of Pangea. (For interpretation of the references to color in this figure legend, the reader is referred to the web version of this article.)

the seafloor is an important feature of our planet because it exhibits a first-order control on e.g. bathymetry, sea level, and planetary cooling through regulation of surface heat flow (i.e. loss of mantle heat). Therefore, as a third benchmark, we compare the time-dependent age-area distributions of the seafloor as generated by our algorithm with those published in Müller et al. (2016).

We observe a clear time-dependence in the age-area distributions computed from our age grids, and this time-dependence is nearly identical to that predicted by M16 (Fig. 6). Given the broad observed trend toward relatively younger seafloor ages between 140–80 Ma, we anticipate that some of these seafloor age variations are related to the widespread development of new ridge systems during the Cretaceous. The initiation of some of these new ridge systems (including the southern mid-Atlantic) was associated with late-stage Pangea breakup, whereas other new ridges appeared in the Paleo-Pacific basin, probably related to the emplacement of large igneous provinces (Torsvik et al., 2019). The rapid development of these new ridges, producing juvenile oceanic lithosphere, must have been synchronously balanced with increased subduction that would have accelerated the destruction of relatively old seafloor. These two processes combined thus explains

the tendency toward relatively younger seafloor during the Cretaceous (Fig. 6).

In summary, our algorithm reproduces detailed reconstructions of seafloor ages like those of M16. We observe only minor regional differences between the algorithm-generated present-day seafloor age grid and the M16 model. These differences mainly occur in regions where Matthews et al. (2016) inferred plate boundary locations that deviate from the interpreted isochrons of M16. This merely demonstrates that our algorithm is an automatic and fast way to detect inconsistencies between data and models. Global features like the age-area distribution, which is important for many geodynamic applications, are robustly reproduced over time. Thus, as plate tectonic reconstructions improve, so will the reliability and regional resolution of the age-grids produced by our algorithm.

3.2. An example application: Paleo sea level

In this section we will demonstrate how our new algorithm and paleo-age grids (computed as described in Section 3.1) can be used to study tectonic mechanisms for sea level variations during the last

400 Myr. We would like to stress that the age-grids generated by our algorithm are bound to the input plate model, and as is the case for all plate models operating in times earlier than 200 Ma, the kinematics of all oceanic plates are necessarily synthetic (because no in situ oceanic lithosphere older than 200 Ma has survived to the present-day). This naturally implies that the construction of age-grids for earlier times is much more uncertain, and interpretation of them should be done with caution and care; here we only use these synthetic age grids to consider some global, first-order trends for the sake of demonstration.

From the generated seafloor age grids, we compute bathymetry by applying the age-depth relation of Crosby and McKenzie (2009) (alternative age-depth relations are explored in Figure S2). Next, we use these bathymetry grids (e.g., Fig. 7C) to compute the change in average ocean basin depth relative to the present-day. To account for temporal changes in sediment thickness (which depend directly on seafloor age as well as on latitude) we follow Straume et al. (2019). Finally, we compare how these changes in ocean depth would affect sea level, and relate them to the sea level history (Fig. 7D) as inferred from the sedimentary record (Hallam, 1992; Haq and Al-Qahtani, 2005; Haq and Schutter, 2008). Although many other processes affect sea level fluctuations on tectonic time scales, the age-area distribution of the seafloor (through thermal subsidence of the ageing oceanic lithosphere) exhibits the first-order control, and is the only process that shows a direct correlation with the sea level record (Müller et al., 2008b; Conrad, 2013; Karlsen et al., 2019a). Therefore, an automatic method for generating seafloor age grids (from which ocean depth can be computed) enables sea level to be used as a first-order order deep-time constraint on plate tectonic reconstructions. A selection of our new seafloor age grids from the Paleozoic, with corresponding bathymetry, is shown in Figure S3.

Our prediction of sea level fluctuations caused by ocean depth changes inferred from our 400 Myr reconstruction of age grids shows a first-order agreement with established sea level records (Hallam, 1992; Haq and Al-Qahtani, 2005; Haq and Schutter, 2008). Such a correlation has been noted previously into the Mesozoic (e.g., Müller et al. 2008b, Conrad 2013), but our algorithm applied to the plate reconstructions of Matthews et al. (2016) shows that this correlation may extend back into the late Paleozoic. Our age models predict a clear peak in sea level during the late stages of Pangea assembly (~ 340 Ma, Fig. 7D), in agreement with the early predictions of sea-level change based on conceptual models of a supercontinental cycle (Worsley et al., 1985, 1986; Nance et al., 1986). Moreover, the consistency between predicted and observed sea level indicates that the tectonic rates (seafloor spreading and its counterpart, seafloor subduction) in the underlying plate tectonic model might be reasonable for this period of time.

3.3. Limitations

The uncertainties in the generated seafloor age grids are directly linked to, and controlled by, the underlying plate tectonic model. Thus, the generated age-grids are dependent on global plate motions and the locations of mid-ocean ridges and subduction zones, for which the assignment of formal errors is impractical to impossible. For these reasons, we expect uncertainty in the age grids to be proportional to those of the underlying plate tectonic reconstructions, with negligible additional uncertainty introduced through the rather straightforward computational steps of our algorithm (Fig. 2). A final word of caution is that the generated age grids will never be better than the input plate model. We thus advise users to familiarize themselves with the uncertainties tied to the underlying plate tectonic reconstructions.

4. Conclusions

The development of plate tectonic reconstructions in the past decade has been rapid, with the introduction of powerful new tools (Boyden et al., 2011; Clark et al., 2012; Gurnis et al., 2012; Wu et al., 2015;

Shephard et al., 2017; Gurnis et al., 2018) and the augmentation of global kinematic datasets (Seton et al., 2014; Gaina and Jakob, 2019) propelling a concomitant proliferation of new and emergent full-plate models, of both regional (Shephard et al., 2013; Zahirovic et al., 2014; Gibbons et al., 2015; Domeier, 2016; Zahirovic et al., 2016; Domeier, 2018; Torsvik et al., 2019) and global scope (Seton et al., 2012; Domeier and Torsvik, 2014; Müller et al., 2016; Matthews et al., 2016; Merdith et al., 2017; Müller et al., 2019). Part of the power of these latest full-plate models is that they implicitly provide information on plate kinematics across the entire global (or regional) surface (Gurnis et al., 2012), and so can be used to derive seafloor age grids to test and evaluate them, as well as to potentially explore other geophysical questions that relate to seafloor ages. Unfortunately, while the information needed to compute seafloor ages is implicitly available, the presently-established workflows to retrieve and process this information are time-consuming, laborious and not publicly available. This emphasizes the need for a method that can automatically generate seafloor age grids from full-plate tectonic reconstructions.

In this study we have presented an algorithm for generating seafloor age grids that robustly reproduces the known present-day ocean floor ages, as well as a previously published model for the time-dependent age-area distribution. This new method has been applied to generate the first set of publicly available oceanic lithosphere age grids that approximate the first order age distribution of late Paleozoic oceans. Application of our generated seafloor models to estimate past sea level changes reveals a general agreement with observations from the sedimentary record (Hallam, 1992; Haq and Al-Qahtani, 2005; Haq and Schutter, 2008), and provides a possible explanation for a peak in sea level during the assembly phase of Pangea. We hope that our automated algorithm will enable such comparisons between age-grid predictions and existing geological constraints to become a routine procedure of the full-plate model development process. Such an improved workflow should ultimately lead to better and more self-consistent combined reconstructions of both plate tectonics and seafloor ages.

Computer code availability

Name of code: Tracer Tectonics (TracTec)

Developer: Krister S. Karlsen (e-mail: k.s.karlsen@geo.uio.no; phone: +47 22 85 40 80).

Year first available: 2019.

Hardware required: No requirements.

Program language: Python 2.7.

Software dependencies: GMT (only post-processing) and the following Python libraries: pyGPlates, scipy, numpy.

Program size: 86 MB (including benchmark age grids)

Source code: <http://doi.org/10.5281/zenodo.3687548>

CRediT authorship contribution statement

Krister S. Karlsen: Formal analysis, Investigation, Methodology, Software, Visualization, Writing - original draft, Writing - review & editing. **Mathew Domeier:** Conceptualization, Formal analysis, Methodology, Writing - original draft, Writing - review & editing. **Carmen Gaina:** Supervision, Conceptualization, Formal analysis, Project administration, Writing - original draft, Writing - review & editing. **Clinton P. Conrad:** Supervision, Conceptualization, Formal analysis, Project administration, Writing - original draft, Writing - review & editing.

Declaration of competing interest

The authors declare that they have no known competing financial interests or personal relationships that could have appeared to influence the work reported in this paper.

Acknowledgments

This paper has benefited from discussions with members of the CEED Earth Modelling group. Additionally, we thank Michael Gurnis and one anonymous reviewer for excellent suggestions that helped improve the algorithm. Calculations in the main algorithm were performed with Python (Van Rossum and Drake, 2011) and pyGPlates, while GMT (Wessel et al., 2013) was used for post-processing. We thank Fabio Cramereri for the development of perceptually uniform and color-vision-deficiency friendly color maps (Cramereri, 2018b), ensuring an accurate representation of the underlying data in the figures (Cramereri, 2018a).

This research was funded by the Research Council of Norway's (RCN) Centres of Excellence Project 223272 and RCN project 250111.

Appendix A. Supplementary data

Supplementary material related to this article can be found online at <https://doi.org/10.1016/j.cageo.2020.104508>.

References

- Becker, T.W., Conrad, C.P., Buffett, B., Müller, R.D., 2009. Past and present seafloor age distributions and the temporal evolution of plate tectonic heat transport. *Earth Planet. Sci. Lett.* 278 (3–4), 233–242.
- Boyden, J.A., Müller, R.D., Gurnis, M., Torsvik, T.H., Clark, J.A., Turner, M., Ivey-Law, H., Watson, R.J., Cannon, J.S., 2011. Next-generation plate-tectonic reconstructions using GPlates.
- Clark, S.R., Skogseid, J., Stensby, V., Smethurst, M.A., Tarrou, C., Bruaset, A.M., Thurmond, A.K., 2012. 4DPlates: On the fly visualization of multilayer geoscientific datasets in a plate tectonic environment. *Comput. Geosci.* 45, 46–51.
- Cogné, J.P., Humler, E., 2004. Temporal variation of oceanic spreading and crustal production rates during the last 180 My. *Earth Planet. Sci. Lett.* 227 (3–4), 427–439.
- Coltice, N., Rolf, T., Tackley, P.J., Labrosse, S., 2012. Dynamic causes of the relation between area and age of the ocean floor. *Science* 336 (6079), 335–338.
- Conrad, C.P., 2013. The solid Earth's influence on sea level. *GSA Bull.* 125 (7–8), 1027–1052.
- Conrad, C.P., Lithgow-Bertelloni, C., 2004. The temporal evolution of plate driving forces: Importance of “slab suction” versus “slab pull” during the Cenozoic. *J. Geophys. Res. Solid Earth* 109 (B10).
- Cramereri, F., 2018a. Geodynamic diagnostics, scientific visualisation and StagLab 3.0. *Geosci. Model Dev.* 11 (6), 2541–2562.
- Cramereri, F., 2018b. Scientific colour-maps. <http://dx.doi.org/10.5281/zenodo.1243862>, Zenodo.
- Cramereri, F., Conrad, C.P., Montési, L., Lithgow-Bertelloni, C.R., 2019. The dynamic life of an oceanic plate. *Tectonophysics* 760, 107–135.
- Crosby, A., McKenzie, D., 2009. An analysis of young ocean depth, gravity and global residual topography. *Geophys. J. Int.* 178 (3), 1198–1219.
- Domeier, M., 2016. A plate tectonic scenario for the Iapetus and Rheic oceans. *Gondwana Res.* 36, 275–295.
- Domeier, M., 2018. Early Paleozoic tectonics of Asia: Towards a full-plate model. *Geosci. Front.* 9 (3), 789–862.
- Domeier, M., Torsvik, T.H., 2014. Plate tectonics in the late Paleozoic. *Geosci. Front.* 5 (3), 303–350.
- Faccenna, C., Becker, T.W., Lallemand, S., Steinberger, B., 2012. On the role of slab pull in the Cenozoic motion of the Pacific plate. *Geophys. Res. Lett.* 39 (3).
- Gaina, C., Jakob, J., 2019. Global eocene tectonic unrest: Possible causes and effects around the North American plate. *Tectonophysics* 760, 136–151.
- Gibbons, A., Zahirovic, S., Müller, R., Whittaker, J., Yatthes, V., 2015. A tectonic model reconciling evidence for the collisions between India, Eurasia and intra-oceanic arcs of the central-eastern Tethys. *Gondwana Res.* 28 (2), 451–492.
- Greiner, B., 1999. Euler rotations in plate-tectonic reconstructions. *Comput. Geosci.* 25 (3), 209–216.
- Gurnis, M., Turner, M., Zahirovic, S., DiCaprio, L., Spasojevic, S., Müller, R.D., Boyden, J., Seton, M., Manea, V.C., Bower, D.J., 2012. Plate tectonic reconstructions with continuously closing plates. *Comput. Geosci.* 38 (1), 35–42.
- Gurnis, M., Yang, T., Cannon, J., Turner, M., Williams, S., Flament, N., Müller, R.D., 2018. Global tectonic reconstructions with continuously deforming and evolving rigid plates. *Comput. Geosci.* 116, 32–41.
- Hallam, A., 1992. *Phanerozoic Sea-Level Changes*. Columbia University Press.
- Haq, B.U., Al-Qahtani, A.M., 2005. Phanerozoic cycles of sea-level change on the Arabian platform. *GeoArabia* 10 (2), 127–160.
- Haq, B.U., Schutter, S.R., 2008. A chronology of Paleozoic sea-level changes. *Science* 322 (5898), 64–68.
- Hays, J.D., Pitman, W.C., 1973. Lithospheric plate motion, sea level changes and climatic and ecological consequences. *Nature* 246 (5427), 18–22.
- Hounslow, M.W., Domeier, M., Biggin, A.J., 2018. Subduction flux modulates the geomagnetic polarity reversal rate. *Tectonophysics* 742, 34–49.
- Karlsen, K.S., Conrad, C.P., Magni, V., 2019a. Deep water cycling and sea level change since the breakup of pangea. *Geochem. Geophys. Geosyst.* 20 (6), 2919–2935.
- Karlsen, K.S., Domeier, M., Gaina, C., Conrad, C.P., 2019b. *TracerTectonics* (Version 2.0). <http://dx.doi.org/10.5281/zenodo.3687548>, Zenodo.
- Loyd, S., Becker, T., Conrad, C., Lithgow-Bertelloni, C., Corsetti, F., 2007. Time variability in Cenozoic reconstructions of mantle heat flow: plate tectonic cycles and implications for Earth's thermal evolution. *Proc. Natl. Acad. Sci.* 104 (36), 14266–14271.
- Matthews, K.J., Maloney, K.T., Zahirovic, S., Williams, S.E., Seton, M., Mueller, R.D., 2016. Global plate boundary evolution and kinematics since the late Paleozoic. *Glob. Planet. Change* 146, 226–250.
- Maunder, B., van Hunen, J., Bouilhol, P., Magni, V., 2019. Modeling slab temperature: A reevaluation of the thermal parameter. *Geochem. Geophys. Geosyst.* 20 (2), 673–687.
- Merdith, A.S., Atkins, S.E., Tetley, M.G., 2019. Tectonic controls on carbon and serpentine storage in subducted upper oceanic lithosphere for the past 320 Ma. *Front. Earth Sci.* 7, 332.
- Merdith, A.S., Collins, A.S., Williams, S.E., Pisarevsky, S., Foden, J.D., Archibald, D.B., Blades, M.L., Alessio, B.L., Armistead, S., Plavs, D., et al., 2017. A full-plate global reconstruction of the Neoproterozoic. *Gondwana Res.* 50, 84–134.
- Müller, R.D., Roest, W.R., Royer, J.-Y., Gahagan, L.M., Sclater, J.G., 1997. Digital isochrons of the world's ocean floor. *J. Geophys. Res. Solid Earth* 102 (B2), 3211–3214.
- Müller, R.D., Sdrorlias, M., Gaina, C., Roest, W.R., 2008a. Age, spreading rates, and spreading asymmetry of the world's ocean crust. *Geochem. Geophys. Geosyst.* 9 (4).
- Müller, R.D., Sdrorlias, M., Gaina, C., Steinberger, B., Heine, C., 2008b. Long-term sea-level fluctuations driven by ocean basin dynamics. *Science* 319 (5868), 1357–1362.
- Müller, R.D., Seton, M., Zahirovic, S., Williams, S.E., Matthews, K.J., Wright, N.M., Shephard, G.E., Maloney, K.T., Barnett-Moore, N., Hosseinpour, M., et al., 2016. Ocean basin evolution and global-scale plate reorganization events since Pangea breakup. *Annu. Rev. Earth Planet. Sci.* 44, 107–138.
- Müller, R.D., Zahirovic, S., Williams, S.E., Cannon, J., Seton, M., Bower, D.J., Tetley, M.G., Heine, C., Le Breton, E., Liu, S., et al., 2019. A global plate model including lithospheric deformation along major rifts and orogens since the Triassic. *Tectonics*.
- Nance, R.D., Worsley, T.R., Moody, J.B., 1986. Post-Archean biogeochemical cycles and long-term episodicity in tectonic processes. *Geology* 14 (6), 514–518.
- Pitman, III, W.C., 1978. Relationship between eustasy and stratigraphic sequences of passive margins. *Geol. Soc. Am. Bull.* 89 (9), 1389–1403.
- Sclater, J., Jaupart, C., Galson, D., 1980. The heat flow through oceanic and continental crust and the heat loss of the Earth. *Rev. Geophys.* 18 (1), 269–311.
- Seton, M., Müller, R., Zahirovic, S., Gaina, C., Torsvik, T., Shephard, G., Talsma, A., Gurnis, M., Turner, M., Maus, S., et al., 2012. Global continental and ocean basin reconstructions since 200 Ma. *Earth-Sci. Rev.* 113 (3–4), 212–270.
- Seton, M., Whittaker, J.M., Wessel, P., Müller, R.D., DeMets, C., Merkouriev, S., Cande, S., Gaina, C., Eagles, G., Granot, R., et al., 2014. Community infrastructure and repository for marine magnetic identifications. *Geochem. Geophys. Geosyst.* 15 (4), 1629–1641.
- Shephard, G.E., Matthews, K.J., Hosseini, K., Domeier, M., 2017. On the consistency of seismically imaged lower mantle slabs. *Sci. Rep.* 7 (1), 10976.
- Shephard, G.E., Müller, R., Seton, M., 2013. The tectonic evolution of the Arctic since Pangea breakup: Integrating constraints from surface geology and geophysics with mantle structure. *Earth-Sci. Rev.* 124, 148–183.
- Sim, S.J., Stegman, D.R., Coltice, N., 2016. Influence of continental growth on mid-ocean ridge depth. *Geochem. Geophys. Geosyst.* 17 (11), 4425–4437.
- Straume, E., Gaina, C., Medvedev, S., Hochmuth, K., Gohl, K., Whittaker, J.M., Abdul Fattah, R., Doornenbal, J., Hopper, J.R., 2019. GlobSed: Updated total sediment thickness in the world's oceans. *Geochem. Geophys. Geosyst.* 20 (4), 1756–1772.
- Torsvik, T.H., Steinberger, B., Shephard, G.E., Doubrovine, P.V., Gaina, C., Domeier, M., Conrad, C.P., Sager, W.W., 2019. Pacific-Panthalassic reconstructions: Overview, errata and the way forward. *Geochem. Geophys. Geosyst.* 20 (7), 3659–3689.
- Van Rossum, G., Drake, F.L., 2011. *The Python Language Reference Manual*. Network Theory Ltd.
- Vine, F.J., Matthews, D.H., 1963. Magnetic anomalies over oceanic ridges. *Nature* 199 (4897), 947–949.
- Wessel, P., Smith, W.H., Scharroo, R., Luis, J., Wobbe, F., 2013. Generic mapping tools: improved version released. *EOS Trans. Am. Geophys. Union* 94 (45), 409–410.
- Worsley, T., Moody, J., Nance, R., 1985. Proterozoic to recent tectonic tuning of biogeochemical cycles. The carbon cycle and atmospheric CO₂: natural variations Archean to present 32, 561–572.
- Worsley, T.R., Nance, R., Moody, J.B., 1986. Tectonic cycles and the history of the Earth's biogeochemical and paleoceanographic record. *Paleoceanography* 1 (3), 233–263.
- Wu, L., Kravchinsky, V.A., Potter, D.K., 2015. PMTec: A new MATLAB toolbox for absolute plate motion reconstructions from paleomagnetism. *Comput. Geosci.* 82, 139–151.
- Zahirovic, S., Matthews, K.J., Flament, N., Müller, R.D., Hill, K.C., Seton, M., Gurnis, M., 2016. Tectonic evolution and deep mantle structure of the eastern Tethys since the latest Jurassic. *Earth-Sci. Rev.* 162, 293–337.
- Zahirovic, S., Seton, M., Müller, R., 2014. The cretaceous and Cenozoic tectonic evolution of Southeast Asia. *Solid Earth* 5 (1), 227.